

Toward Wideband Steerable Acoustic Metasurfaces with Arrays of Active Electroacoustic Resonators

Hervé Lissek,^{1, a)} Etienne Rivet,¹ Thomas Laurence,¹ and Romain Fleury²

¹⁾*Ecole Polytechnique Fédérale de Lausanne, Laboratory of Signal Processing 2, EPFL STI IEL LTS2, Station 11, CH-1015 Lausanne, Switzerland.*

²⁾*Ecole Polytechnique Fédérale de Lausanne, Laboratory of Wave Engineering, EPFL STI IEL LWE, Station 11, CH-1015 Lausanne, Switzerland.*

(Dated: 9 January 2018)

We introduce an active concept for achieving acoustic metasurfaces with steerable reflection properties, effective over a wide frequency band. The proposed active acoustic metasurface consists in a surface array of subwavelength loudspeakers diaphragms, each with programmable individual active acoustic impedances allowing for local control over the different reflection phases over the metasurface. The active control framework used for controlling the reflection phase over the metasurface is derived from the Active Electroacoustic Resonator concept. Each unit-cell simply consists of a current-driven electrodynamic loudspeaker in a closed box, whose acoustic impedance at the diaphragm is judiciously adjusted by connecting an active electrical control circuit. The control is known to achieve a wide variety of acoustic impedances on a single loudspeaker diaphragm used as an acoustic resonator, with the possibility to shift its resonance frequency by more than one octave. The paper presents a methodology for designing such active metasurface elements. An experimental validation of the achieved individual reflection coefficients is presented, and full wave simulations present a few examples of achievable reflection properties, with a focus on the bandwidth of operation of the proposed control concept.

PACS numbers: 43.20.El, 43.20.Tb, 43.38.Hz

Keywords: Active acoustic metasurface, adjustable reflectarray, electroacoustic resonators, active acoustic impedance control

^{a)}Electronic mail: herve.lissek@epfl.ch

INTRODUCTION

31 Acoustic Metasurfaces (AMS) designate surface arrangements of subwavelength unit-cells
32 that are engineered so as to artificially reshape wavefronts out of an impinging sound pres-
33 sure field, owing to a prescribed variation of local acoustic properties. They are essentially
34 envisaged as interfaces with exogenous propagating media, whereas Acoustic Metamaterials
35 (AMM) rather refer to wave manipulations within the artificial medium¹ (although connec-
36 tion with an external medium are also envisaged in Leaky-Wave Antenna applications^{2,3}).
37 Metasurfaces can then be designed to reflect wavefronts in an anomalous manner (“re-
38 flectarray”), with potential application to acoustic cloaking^{4,5}, or for sound transmission
39 manipulation (“transmit-array”)⁶ with application to acoustic lensing. They can also be
40 applied to sound channelling^{7,8} and sound absorption⁹.

41 The manipulation of acoustic wavefronts in a reflectarray is achieved by adequately dis-
42 tributing the phase of the reflection coefficient over the metasurface. Several concepts have
43 been investigated to artificially control the reflection phase of a unit-cell, while remaining
44 small with respect to the wavelength. Spiral acoustic unit-cells have been proposed, allowing
45 lengthening the acoustic path through a labyrinthine-type channel inside the unit-cell^{5,10}.
46 Helmholtz resonators are also obvious solutions, since their resonance frequency can be tuned
47 by tailoring their cavity and neck dimensions. By selecting gradually varying Helmholtz
48 resonances, the reflection coefficient phase can be adjusted to a target distribution^{11,12}. Al-
49 ternatively, membrane-type acoustic metasurfaces have been proposed achieving acoustic
50 impedance gratings either by adequate spacing between membranes¹³, or by adapting the
51 membrane thicknesses⁴. Such passive AMS concepts have been thoroughly investigated to
52 derive design guidelines and assess their performance mostly at a computational stage. Some
53 studies have reported practical realization of acoustic metasurfaces. Besides the application
54 to cloaking¹¹, a recent paper of Jimenez et al¹² reports the design of an acoustic meta-
55 surface based on stacked coupled Helmholtz resonators, that allows achieving controllable
56 sound diffusion for use in room acoustics. Meanwhile, passive AMS suffer from drastic lim-
57 itations: they are inherently narrow-band at a prescribed frequency due to their resonant
58 behaviour¹⁴, and they cannot be reconfigured in real-time. Since the properties of the AMS
59 are fixed by design (geometry and material properties), it makes passive AMS concepts irrel-
60 evant to most practical acoustic problems, with respect to bandwidth and reconfigurability.

This motivated the development of a new class of AMS implementing active unit-cells concepts, such as piezoelectric membranes with dedicated feedback-control units, allowing for real time reconfiguration of a metamaterial slab to achieve prescribed lensing properties¹⁵. Alternatively, an active acoustic metasurface (AAMS) concept implementing a spatial arrangement of unit-cells, composed of a membrane with an attached magnetic mass actuated by an electromagnetic transducer, has been proposed to allow reflection reconfigurability¹⁶. Although the literature on active acoustic metasurfaces mainly addresses reconfigurability aspects, the possibility to extend the control bandwidth has been less investigated, due to a lack of stable broadband active control concepts.

The concept of Active Electroacoustic Resonators (AER), firstly developed for achieving broadband sound absorption in the low-frequency range^{17–20}, may represent an interesting solution to this problem by providing an adjustable and/or broadband unit-cell for AAMS applications^{21–23}. The control scheme at work in such AER assigns a target acoustic impedance to the diaphragm of the current-driven loudspeaker, through a sensor-/shunt-based impedance control¹⁹. With this techniques, a same Electroacoustic Resonator can be dynamically tuned to a wide range of resonance frequencies or quality factors, through a somehow simple control law. Since the manipulation of wavefronts at the heart of the AMS concept requires assigning prescribed acoustic impedances to the unit-cells, and since it can be achieved on a broadband manner with AER, it is expected to overcome the usual limitations (eg. bandwidth) of the passive AMS concepts reported so far in the literature.

In this paper, the concept of an AAMS composed of a 2D arrangement of subwavelength AER is introduced aiming at achieving broadband and steerable (reconfigurable) anomalous reflection. The first section reminds the general properties of the proposed AMS framework, with a focus on the control parameters over the metasurface allowing the reflection direction for a given incident plane wave. In the second section, the AER concept is presented. Then a methodology is introduced that sets unit-cells controllers in order to achieve the prescribed reflection properties, followed by an experimental validation of the achieved acoustic properties. Finally, a few examples of reflectarray settings will be discussed, based on simulations with a commercial finite-elements software (COMSOL Multiphysics).

MEMBRANE-TYPE ACOUSTIC METASURFACE

91 A. Description of the proposed Acoustic Metasurface

92 The proposed AMS consists of subwavelength unit-cells spatially arranged over a planar
 93 lattice (over the “horizontal” plane xOy), aiming at controlling the reflected wavefronts for
 94 any arbitrary incident plane waves. The subwavelength condition imposes that the lattice
 95 constant $d_d < \frac{\lambda_{max}}{10}$, where $\lambda_{max} = \frac{c_0}{f_{max}}$ is the wavelength corresponding to the upper
 96 working frequency f_{max} , with $c_0 = 343 \text{ m.s}^{-1}$ the sound celerity in the air. We denote the
 97 reflection coefficient by $\Gamma(x, y)$ at each point (x, y) over the AMS, and its phase by $\psi(x, y)$.
 98 Any incident [respectively reflected] plane wave will be characterized in the following by its
 99 wave-vector $\vec{k}_i (\cos(\phi_i), \sin(\phi_i), \cos(\theta_i))$ [respectively $\vec{k}_r (\cos(\phi_r), \sin(\phi_r), \cos(\theta_r))$], where ϕ_i
 100 [respectively ϕ_r] is the azimuth over the AMS plane and θ_i [respectively θ_r] the elevation of
 101 the incident [respectively reflected] plane wave vector.

102 According to Ref.⁴, in order to prescribe the wave-vector k_r of the reflected wave for a
 103 given wave-vector k_i of the incident wave, at given frequency f , the reflection phase gradient
 104 $\vec{\nabla}\psi(x, y)$ should satisfy:

$$\frac{\partial\psi}{\partial x} = -\frac{2\pi f}{c_0} (\sin\theta_r \cos\phi_r + \sin\theta_i \cos\phi_i), \quad (1a)$$

$$\frac{\partial\psi}{\partial y} = -\frac{2\pi f}{c_0} (\sin\theta_r \sin\phi_r + \sin\theta_i \sin\phi_i). \quad (1b)$$

105 These conditions can also be formulated for a discrete arrangement of subwavelength
 106 reflectors. We now consider the 2D arrangement of small identical circular pistons of radius
 107 r_d over the AMS plane as illustrated in Figure 1. In this configuration, we consider the
 108 regular lattice directions x and y with a same lattice constant $d_d = 2r_d$, so that the
 109 center of each disk is located at (x_0^m, y_0^n) with $x_0^m = (m - 1)d_d + x_0$ and $y_0^n = (n - 1)d_d + y_0$,
 110 and (x_0, y_0) the position of the first cell of the lattice. The subwavelength conditions then
 111 imposes that $r_d < \frac{c_0}{20 f_{max}}$, which corresponds to a maximum disk radius of about 34 mm at
 112 500 Hz.

113 Each disk, denoted by the couple (m, n) over the x and y axes should then present the
 114 following reflection phase:

115

resonance frequency f_s and quality factor Q_s defined as:

$$r_s = \frac{R_{as}}{Z_c}, \quad (4a)$$

$$f_s = \frac{1}{2\pi\sqrt{M_{as}C_{as}}}, \quad (4b)$$

$$Q_s = \frac{1}{R_{as}}\sqrt{\frac{M_{as}}{C_{as}}}, \quad (4c)$$

where $Z_c = \rho_0 c_0$ is the characteristic impedance of the air, and $\rho_0 = 1.2 \text{ kg.m}^{-3}$ the mass density of the air.

The reflection coefficient, under normal incidence, of a resonator of impedance $Z_a(\omega)$ is defined as: $\Gamma(\omega) = \frac{Z_a(\omega) - Z_c}{Z_a(\omega) + Z_c}$. According to Eq.3, it can then be derived as:

$$\begin{aligned} \Gamma(\omega) &= \frac{(R_{as} - Z_c) + j\left(\omega M_{as} - \frac{1}{\omega C_{as}}\right)}{(R_{as} + Z_c) + j\left(\omega M_{as} - \frac{1}{\omega C_{as}}\right)} \\ &= \frac{-\left(\frac{\omega}{\omega_s}\right)^2 + j\left(\frac{\omega}{\omega_s}\right)\frac{1}{Q_s}\left(1 - \frac{1}{r_s}\right) + 1}{-\left(\frac{\omega}{\omega_s}\right)^2 + j\left(\frac{\omega}{\omega_s}\right)\frac{1}{Q_s}\left(1 + \frac{1}{r_s}\right) + 1}. \end{aligned} \quad (5)$$

Finally, the reflection phase follows:

$$\begin{aligned} \psi(\omega) &= \tan^{-1}\left(\frac{2Z_c\left(\omega M_{as} - \frac{1}{\omega C_{as}}\right)}{R_{as}^2 - Z_c^2 + \left(\omega M_{as} - \frac{1}{\omega C_{as}}\right)^2}\right) \\ &= \tan^{-1}\left[\frac{2\left(\frac{\omega}{\omega_s}\right)^3 - \left(\frac{\omega}{\omega_s}\right)}{r_s Q_s \left(\frac{\omega}{\omega_s}\right)^4 + \left(\frac{\omega}{\omega_s}\right)^2 \left[\frac{1}{Q_s^2}\left(1 - \frac{1}{r_s^2}\right) - 2\right] - 1}\right]. \end{aligned} \quad (6)$$

The inspection of Eq. 6 shows that the proper selection of the mechanical resonator parameters (M_{ms}, R_{ms}, C_{ms}) (or (r_s, f_s, Q_s)) allows adjusting the reflection phase spanning at any given frequency. However, the achievable phase range over a given frequency bandwidth may vary depending on the resonator characteristics, especially its quality factor and loss factor, namely the value of r_s . In particular, the achievable phase range is limited to less than $[-\frac{\pi}{2}, \frac{\pi}{2}]$ for $r_s \geq 1$, which disqualifies such values for spanning the whole unit circle. Therefore, the design of the resonators array is constrained by the selection of Q_s and r_s . In Appendix A, we demonstrate that two important criteria must be considered: first, the mechanical

144 distance should be chosen so that $r_s < 1$, for example $R_{ms} = \frac{1}{3}S_dZ_c$, in order to allow
 145 the reflection phase varying linearly within the broadest frequency band, while spanning a
 146 wide range of values within $[0, 2\pi]$; secondly, the resonator quality factor Q_s should neither
 147 be too high, since the assumption of linear phase is valid over a limited frequency band
 148 only, nor too low since the phase variation may not cover sufficient values within one octave.
 Therefore, the following mechanical resonator values will be considered in the following:

$$R_{ms} = \frac{Z_c S_d}{3}, \quad (7a)$$

$$Q_s = 6. \quad (7b)$$

149 The metasurface illustrated in Figure 1 could be theoretically achieved by properly de-
 150 signing discrete passive mechanical resonators presenting the reflection phase grating of Eq.
 151 2 at least over one octave around a desired central frequency f_0 . For that, we could tune the
 152 resonance frequency of each unit-cell to a given value f^{mn} so that their individual reflection
 153 phase at f_0 matches the one targeted on Eq. 2, with the constraints of Eq. 7. However,
 154 it is impossible to ensure in practice such variations of mechanical resistance, resonance
 155 frequency and quality factor over the whole $M \times N$ unit-cells.

156 Instead, we propose an active acoustic impedance control strategy to adjust the acoustical
 157 properties of the unit-cells along the metasurface. Indeed, it appears to be a more elegant
 158 manner than passive construction, potentially allowing for full reconfigurability over a broad
 159 bandwidth (at least over one octave). In this paper, the proposed unit-cell concept is
 160 realized with a subwavelength Active Electroacoustic Resonator (AER) concept. The control
 161 principle consists in actively tuning the different AER with indices (m, n) to the target
 162 resonance frequencies f^{mn} , with a view to shifting their reflection phases $\arg(\Gamma(f_0))$ at f_0 to
 163 the prescribed values ψ^{mn} , with a constrained resistance and quality factor. The latter should
 164 ensure that the targeted phase grating still holds true over a sufficiently wide frequency band
 165 (namely one octave around f_0), assuming a linear phase variation around f_0 , according to
 166 Appendix A. This means the parameters varied by control should be the passive acoustic
 167 mass M_{as} and compliance C_{as} (supposedly the same over the metasurface without control),
 168 with a resistance set to $\frac{1}{3}Z_c$ for all cells. The following section presents this concept and its
 169 application to the acoustic metasurface.

FIG. 2. Description of the AER concept.

170 III. ACTIVE ELECTROACOUSTIC UNIT-CELLS

171 A. Acoustic impedance control principle

172 Active Electroacoustic Resonators (AER) designate acoustic resonators that can be tuned
 173 or modified through electroacoustic control schemes^{17–19}. AER can especially be achieved
 174 with a control scheme, employing a conventional closed-box electrodynamic loudspeaker di-
 175 aphragm, the acoustic impedance of which can be controlled through a microphone sensing
 176 the total sound pressure p_t in front of the diaphragm, a controller characterized by the trans-
 177 fer function $\Theta(\omega)$ and a transconductance amplifier¹⁹, as illustrated in Figure 2. The volume
 178 of free air in the enclosure is denoted V_b , and the loudspeaker diaphragm is assimilated to a
 179 single-degree of freedom mechanical resonator with parameters (M_{ms}, R_{ms}, C_{mc}) , where C_{mc}
 180 accounts both for the free compliance C_{ms} and the additional compliance due to the vol-
 181 ume of compressible air V_b inside the enclosure²⁵. We can as well define the corresponding
 182 acoustic resonator parameters (M_{as}, R_{as}, C_{ac}) , as in section II B. Last, the electrodynamic
 183 force factor $B\ell$ designates the transduction coefficient of the loudspeaker driver.

184 If we denote $Z_{as}(\omega) = j\omega M_{as} + R_{as} + \frac{1}{j\omega C_{ac}}$ the “passive” acoustical impedance of the
 185 closed-box loudspeaker, $v_d(\omega)$ the diaphragm velocity, and $i(\omega) = \Theta(\omega)p_t(\omega)$ the electrical
 186 current circulating through the loudspeaker coil, then the electroacoustic dynamics of the
 187 AER can be described in the frequency domain as:

$$188 \quad Z_{as}(\omega)v_d(\omega) = p_t(\omega) \left(1 - \frac{B\ell}{S_d}\Theta(\omega) \right) \quad (8)$$

189 The active acoustic impedance Z_a achieved at the loudspeaker diaphragm by the control
 190 can be easily derived from Eq. 8 as¹⁹:

$$191 \quad Z_a(\omega) = \frac{p_t(\omega)}{v_d(\omega)} = \frac{Z_{as}(\omega)}{1 - \frac{B\ell}{S_d}\Theta(\omega)} \quad (9)$$

192 Thus, a target frequency-dependent acoustic impedance $Z_{at}(\omega)$ can be chosen, and as-
 193 signed to the diaphragm if the controller is set to the target transfer function:

$$194 \quad \Theta_t(\omega) = \frac{S_d}{B\ell} \frac{Z_{at}(\omega) - Z_{as}(\omega)}{Z_{at}(\omega)} \quad (10)$$

Target acoustic impedance

196 Let us now chose the target acoustic impedance $Z_{at}^{mn}(\omega)$ of the (m,n) unit-cell of the
 197 AMS as the one of a single-degree of freedom resonator, that eventually differs from
 198 the passive loudspeaker diaphragm. For that, we will introduce adjustable coefficients
 199 $(\mu_M(m,n), \mu_R(m,n), \mu_C(m,n))$ that will apply to the mass, resistance and compliance of
 200 each unit-cell (m,n) , so that:

$$201 \quad Z_{at}^{mn}(\omega) = j\omega\mu_M(m,n)M_{as} + \mu_R(m,n)Z_c + \frac{1}{j\omega\mu_C(m,n)C_{ac}}, \quad (11)$$

202 where the new resonance frequency of this active acoustic resonator is $f^{mn} = \frac{1}{\sqrt{\mu_M(m,n)\mu_C(m,n)}}f_s$.

203 The controller transfer function should then be set to:

$$204 \quad \Theta_t^{mn}(\omega) = \frac{S_d}{Bl} \frac{(j\omega)^2 M_{as} (\mu_M(m,n) - 1) + j\omega (\mu_R(m,n) Z_c - R_{as}) + \left(\frac{1 - \mu_C(m,n)}{\mu_C(m,n) C_{ac}} \right)}{(j\omega)^2 \mu_M(m,n) M_{as} + j\omega \mu_R(m,n) Z_c + \frac{1}{\mu_C(m,n) C_{ac}}} \quad (12)$$

205 The control principle introduced at the end of Section II B then consists in identifying the
 206 coefficient pair $\mu_M(m,n)$ and $\mu_C(m,n)$ ($\mu_R(m,n)$ being fixed to 1/3) for each unit-cell (m,n)
 207 of the AMS, allowing shifting the resonance frequency from f_s to a target (active) resonance
 208 frequency f^{mn} , defined in the next section. The next section introduces a methodology for
 209 setting these coefficients, with the aim of achieving desired anomalous reflection angle (ϕ_r, θ_r)
 210 for a given incidence (ϕ_i, θ_i) , over at least one octave around a given central frequency f_0 .

211 IV. ACTIVE ACOUSTIC METASURFACE

212 A. Parametrization of the Active Unit-Cells

213 We will consider an AMS consisting of an array of $M \times N$ small commercially-available
 214 electrodynamic loudspeaker (Monacor SPX-30M, whose Thiele-Small parameters of which
 215 are given in Table I). Their radius $r_d \approx 32$ mm limits the frequency range of operation as
 216 metasurface unit-cells to $f_{max} = 500$ Hz. Moreover, we will consider $\phi_r = \phi_i = 0 \pmod{\pi}$,
 217 yielding an impedance grating only over the x dimension. Under this assumption, the space-
 218 dependence along y collapses, and the acoustic impedance of each AER within a same row
 219 m will be controlled to achieve the target reflection phase:

$$\psi^m(f_0) = -\frac{2\pi f_0}{c_0}(2r_d)m(\sin\theta_r + \sin\theta_i) + \psi_0 \quad (13)$$

The following presents a simple methodology to assign a target reflection angle θ_r for a given incident angle θ_i , at a given central frequency f_0 , with a metasurface of lattice constant $2r_d$. By using the control law of Eq. 12, the acoustic impedance of each unit-cell m over the metasurface will be simply shifted in frequency so that the reflection phase at f_0 matches a target value $\psi^m(f_0)$, following Eq. 13.

We also impose the phase of the $(M/2+1)^{\text{th}}$ cell $\psi^{M/2+1}(f_0) = -\pi$, so that the whole metasurface phases may vary within $[-2\pi; 0]$. Under these conditions, there exists only one frequency f^m for which the phase of the reflection coefficient of the $(M/2+1)^{\text{th}}$ cell matches the target value ψ^m : $\arg(\Gamma^{M/2+1}(f^m)) = \psi^m \pmod{2\pi}$.

Figure 3, represents the reflection phase $\arg(\Gamma^{M/2+1}(f))$ analytically computed in Matlab with Eq.6, corresponding to the acoustic impedance of the $(M/2+1)^{\text{th}}$ cell $Z_{at}^{M/2+1}(\omega)$ defined in Eq.11, with $\mu_M(M/2+1) = \mu_C(M/2+1) = 1$ and $\mu_R(M/2+1) = 1/3$. The different values of ψ^m drawn as round markers on Figure 3 are defined for an array size $M = 32$, for the reflection case $\theta_i = -\frac{\pi}{4}$ and $\theta_r = \frac{\pi}{3}$. Assuming a linear phase variation of the reflection coefficient Γ around f_0 , the target reflection phase $\arg(\Gamma^m(f_0))$ can be achieved at f_0 on cell m by shifting the resonance frequency of the m^{th} active AER by a value $\Delta f^m = f_0 - f^m$. This is finally done by assigning:

$$\mu_M(m) \cdot \mu_C(m) = \left(\frac{f_0}{f^m}\right)^2, \quad (14)$$

while preserving the resonance quality factor $Q_s = 6$ and resistance $R_{as} = \frac{1}{3}Z_c$, as explained in Appendix A. Finally, the coefficients can be identified as:

$$\mu_R(m) = \frac{1}{3} \quad (15a)$$

$$\mu_C(m) = \frac{1}{2\pi Z_c C_{ac} Q_s} \frac{1}{(f_0 + \Delta f^m) \mu_R(m)} \quad (15b)$$

$$\mu_M(m) = \frac{Z_c Q_s}{2\pi M_{as}} \frac{\mu_R(m)}{(f_0 + \Delta f^m)} \quad (15c)$$

Then, the impedance of each cell within row m is assigned thanks to the individual control law $\Theta_t^m(\omega)$, as in Eq. 12. The methodology for designing the AMS can then be

FIG. 3. Reflection phase to prescribe to the 17th cell within a metasurface with $M=32$ rows, computed for the case $(\theta_i = -\frac{\pi}{4}, \theta_r = \frac{\pi}{3})$, imposing a quality factor $Q_s=16$ and resistance factor $\mu_R = 1/3$ (blue line). Identification of the target reflection phases (round markers) and corresponding resonance shifts $\Delta f^m = f_0 - f^m$.

FIG. 4. Blue circles: Achieved reflection coefficients at $f_0 = 343$ Hz with $M=32$ rows (top: amplitude; bottom: phases). Comparison to the targeted values ψ^m (black dotted line).

243 summarized as follows:

244

- 245 1. choice of the target reflected angle θ_r for a given incident angle θ_i (at frequency f_0);
- 246 2. definition of the reflection phase grating ψ^m over the metasurface of lattice constant
- 247 $2r_d$ according to Eq.13;
- 248 3. definition of the reflection phase reference at the $(M/2+1)^{\text{th}}$ cell such as $\arg(\Gamma^{M/2+1}(f_0)) =$
- 249 $-\pi$;
- 250 4. identification of the resonance shift $\Delta f^m = f_0 - f^m$ for each cell over the metasurface,
- 251 so that $\arg(\Gamma^{M/2+1}(f^m)) = \psi^m$;
- 252 5. identification of the control parameters $\mu_M(m)$, $\mu_C(m)$ and μ_R achieving such reso-
- 253 nance shift (Eq. 15);
- 254 6. modification of the acoustic impedance of the m^{th} cell with the controller $\Theta_t^m(\omega)$ of
- 255 Eq.12.

256 Figure 4 shows an example of the reflection coefficient targeted at $f_0 = 343$ Hz on each

257 cell m for an array size $M = 32$, for the reflection case $(\theta_i = -\frac{\pi}{4}, \theta_r = \frac{\pi}{3})$. Figure 5 presents

258 the bode diagrams of the 32 reflection coefficients $\Gamma^m(\omega)$ that can be achieved on the 32

259 cells of the AMS, analytically computed in Matlab from Eq. 5, with the target impedances

260 $Z_{at}^m(\omega)$ defined in Eq.11.

FIG. 5. Rainbow-coloured lines: target reflection coefficients of the 32 unit-cells (from cell #1 in blue to cell #32 in red) of the metasurface, for $\theta_i = -\pi/4$ and $\theta_r = \pi/3$ (top: amplitude, bottom: phase), computed in Matlab with Eq.5. Comparison to the reflection coefficient of the passive Electroacoustic Resonator (black lines).

TABLE I. Measured Thiele-Small parameters of the MONACOR SPX-30M loudspeaker.

Parameter	Symbol	Value	Unit
Effective piston area	S_d	32	cm ²
Mechanical mass	M_{ms}	3.17	g
Mechanical resistance	R_{ms}	0.75	N.s.m ⁻¹
Mechanical compliance (with enclosure)	C_{mc}	184.10 ⁻⁶	m.N ⁻¹
Force factor	$B\ell$	3.67	N/A
Resonance frequency	f_s	208	Hz
Quality factor	Q_s	5.5	

261 B. Experimental Assessment of the Unit-Cells

262 The target reflection coefficients have been programmed on a unit-cell prototype, con-
 263 sisting of a MONACOR SPX-30M loudspeaker in a small wooden enclosure. The Thiele-
 264 Small parameters²⁵ of the closed-box loudspeaker are estimated, following the methodology
 265 proposed by Seifel et al.²⁶, in an impedance tube from two measurements of the acoustic
 266 impedance at the diaphragm, first with the loudspeaker terminals in open circuit, and then
 267 in short circuit (more details are provided in Ref.²⁷, pp. 50-52). The loudspeaker diaphragm
 268 is excited by an exogenous sound source located at the other end of the duct with broadband
 269 noise. The acoustic radiation impedance of the loudspeaker under test, which depends on the
 270 environment in which it is located, has been taken into account in the acoustic impedance
 271 Z_{as} to avoid numerous annotations. These parameters are presented in Table I.

272 The reflection coefficient of the unit-cell prototype diaphragm, mounted in a custom-
 273 made impedance tube, is assessed according to the two-microphones methods described in
 274 ISO 10534-2 standard²⁸. The transfer functions H_{12} between microphones 1 and 2 positions
 275 along the tube are processed through a Multichannel Analyzer (Bruel & Kjaer Pulse Type
 276 3160), and the reflection coefficient of the diaphragm can be derived.

277 On the Active Electroacoustic Resonator side, the total pressure p_t used in the control is
 278 sensed with a PCB 130D20 microphone, located at 5 mm from the electroacoustic absorber
 279 membrane and close to the lateral duct wall of the impedance tube as depicted in Fig.

FIG. 6. Scheme of the experimental setup. The control implementation is depicted in the right-hand side including the microphone, the digital controller and the transconductance amplifier.

FIG. 7. Rainbow-coloured dotted lines: measured achieved reflection coefficient (top: amplitude, bottom: phase) of the 32 unit-cells (from cell #1 in blue to cell #32 in red) of the metasurface, for $\theta_i = -\pi/4$ and $\theta_r = \pi/3$. Comparison to the reflection coefficient measured on the passive Electroacoustic Resonator (black dotted lines).

6. Each transfer function $\Theta_t^{mn}(\omega)$ given by Eq.(12) and (15) applied to the corresponding cell is discretized into an infinite impulse response filter using the Tustin method, then is implemented onto a real-time National Instruments CompactRIO platform supporting field-programmable gate array (FPGA) technology. The voltage signal from the microphone is then digitally converted at a sampling frequency of 80 kHz thanks to an analog module NI 9215, and the output filtered signal u_{out} is delivered by an analog module NI 9263. The overall time delay of the controller (ADC/FPGA/DAC) is equal to 20.6 μ s. A voltage controlled current source, involving an op-amp based improved Howland current pump circuit as illustrated in Fig.6, has to be implemented downstream the digital controller, so that to properly drive the voice-coil loudspeaker in current. The details of the digital controller implementation can be found in Ref.¹⁹ and Ref.²⁷ (pp. 57-58), and more information about the stability and control limitations of the acoustic impedance control can be found in Ref.²⁷ (pp. 73-81).

Figure 7 shows the reflection coefficients measured on the unit-cell prototype, for each of the 32 control settings. The results are compared to the passive reflection coefficient of the unit-cell. We can see that the targeted reflection coefficients are actually achieved with the proposed unit-cell and control framework. Moreover, it is noticeable in this example that the passive resonance frequency is one octave lower than the highest active resonance frequency of the 32 unit-cells, which shows the range of tunability of the control framework.

V. RESULTS AND DISCUSSION

Once the target reflection coefficients have been verified experimentally, the metasurface is numerically modelled on a commercial Finite-Elements Software (COMSOL Multiphysics

303 physics, considering periodic conditions over the y axis, thus limiting the metasurface to a
304 single line of $M = 32$ circular disks of radius r_d , regularly dispatched along the x axis (with
305 lattice constant $2r_d$). The considered propagating domain is then a half-cylinder (symmetry
306 axis along y) of radius $L = 6$ m (including a Perfectly Matched Layer), and height $2r_d$ (to
307 ensure the same lattice constant over y). Each lateral sides of the cylinder are assigned
308 “Sound Hard Boundary” conditions. Each disk representing an AER on the xy plane is
309 assigned an acoustic impedance boundary condition, which is defined as in Eq.11 considering
310 the control parameters of Eq.15, and the remaining area on the xy plane is considered
311 perfectly absorbent (impedance matching condition). We also consider a tetrahedral meshing
312 inside the propagating domain, with mesh size corresponding to 6 nodes per wavelength at
313 450 Hz. A refinement of the mesh is also processed at the level of the metasurface elements,
314 with an additional triangular meshing (refinement by a factor 10 along x and y axes).
315 The “Background Pressure Field” is finally employed to impose an incident plane wave with
316 wave vector $(\cos(\theta_i), 0, \sin(\theta_i))$ and amplitude 1 Pa. In this paper, we will consider the
317 incident plane wave fields impinges the metasurface with incident angle $\theta_i = -\frac{\pi}{4}$ rad, and
318 two reflection cases:

- 319 • $\theta_r = \frac{\pi}{3}$ rad, corresponding to an augmentation of the reflected angle,
- 320 • $\theta_r = 0$ rad, corresponding to a diminution of the reflected angle.

321 Figures 8 and 9 represent the reflected sound pressure levels maps over the xz plane,
322 processed by full-wave simulations, for the two studied cases, at $f = 350$ Hz. It can be seen
323 that the acoustic impedance imposed on the metasurface unit-cells actually allows steering
324 the wavefronts toward the prescribed angle. Since the reflection coefficient amplitude of the
325 whole metasurface unit-cells range between 0.5 and 0.6 at f_0 (as can be seen for example on
326 Figure 4), an expected attenuation of the reflected energy is observed.

327 Figures 10 and 11 present the directivity of the metasurface, namely a polar representation
328 of the normalized sound pressure levels (referred to the maximal value), processed by full-
329 wave simulations at a distance $r = 3$ m from the metasurface center, for both reflection cases
330 ($\theta_r = \frac{\pi}{3}$ rad, and $\theta_r = 0$ rad) and at different frequencies (200 Hz - 250 Hz - 350 Hz and
331 400 Hz). First, the limited size of the AMS (2 meters long) with respect to the studied

FIG. 8. Reflected sound pressure levels (dB re. 20 μ Pa) obtained by full-wave simulations with 32x32 unit-cells, at $f = 350$ Hz, for $\theta_i = -\frac{\pi}{4}$ rad. and $\theta_r = \frac{\pi}{3}$ rad.

FIG. 9. Reflected sound pressure levels (dB re. 20 μ Pa) obtained by full-wave simulations with 32x32 unit-cells, at $f = 350$ Hz, for $\theta_i = -\frac{\pi}{4}$ rad. and $\theta_r = 0$ rad.

332 wavelength explains the occurrence of side lobes. We can also observe that the beam widths
333 depend on frequency. Finally, it seems that the beam shapes are much more spread over
334 angles for the case $\theta_r = \frac{\pi}{3}$ rad than the case $\theta_r = 0$ rad, which can be explained by the
335 fact that the 32 cells span a smaller range of reflection phases over $[-2\pi - 0]$ in the first
336 case. This could be alleviated by designing an AMS with a higher number of unit-cells. But
337 in general, there is a good agreement between the achieved directivities and the targeted
338 reflected angles, which confirm the effectiveness of the AER to achieve a coherent steering
339 over a relatively wide frequency band (almost one octave around 350 Hz).

340 VI. CONCLUSIONS

341 We have proposed Active Electroacoustic Resonators as unit-cells within an acoustic
342 metasurface, in a reflectarray application. The reflection properties have been derived to
343 define individual control laws to assign to each AER unit-cells. The identified control settings
344 have been applied to a conventional electrodynamic loudspeaker in a view to assessing the
345 feasibility of the targeted reflection phases along a metasurface of 32 elements. Then Full-
346 Wave simulations have been processed to simulate the achieved reflection properties with
347 the targeted control settings, showing the effectiveness of the concept for steering wavefronts
348 in a prescribed manner. Moreover, we have shown the effectiveness of the control over a
349 relatively wide frequency band, opening the way to actual applications as reflectarray for
350 audible sounds. Further developments should focus on designing an actual prototype of

FIG. 10. Reflection directivities (polar representation of reflected sound pressure levels in dB referred to the maximal value) obtained by full-wave simulations with 32x32 unit-cells, at frequencies $f = \{250, 300, 350, 400\}$ Hz, for $\theta_i = -\frac{\pi}{4}$ rad. and $\theta_r = \frac{\pi}{3}$ rad.

Fig. 11. Reflection directivities (polar representation of reflected sound pressure levels in dB referred to the maximal value) obtained by full-wave simulations with 32x32 unit-cells, at frequencies $f = \{250, 300, 350, 400\}$ Hz, for $\theta_i = -\frac{\pi}{4}$ rad. and $\theta_r = 0$ rad.

351 metasurface with a hardware allowing individually controlling 32 unit-cells. It is likely to
352 demonstrate the actual performance of the concept, owing to a ad hoc experimental setup
353 to be developed.

354 The proposed methodology for controlling the reflection coefficient phase over the meta-
355 surface is based on the assumption of a linear phase variation, over a large bandwidth around
356 the central frequency f_c . This simplistic assumption is somehow limiting, both in terms of
357 achievable reflection phases than in terms of accurate phase grating over the surface. Other
358 methodologies based on more complex acoustic impedance control strategies, such as Ac-
359 tive Multiple-Degrees-Of-Freedom Electroacoustic Resonators, coupled with an optimization
360 procedure as proposed in Ref.²⁰, could also help improving the concept.

361 ACKNOWLEDGMENTS

362 The authors wish to thank Hussein Esfahlani for the advices on the design of the acoustic
363 metasurface in the COMSOL Multiphysics environment.

364 Appendix A: Discussion on the choice of a passive resonator

365 We consider a single-degree of freedom resonator (r, m, c) , the normalized impedance of
366 which reads

$$367 z = \frac{Z_a}{Z_c} = j\omega m + r + \frac{1}{j\omega c}.$$

368 We also define its resonance frequency $\omega_s = \sqrt{mc}^{-1}$ and quality factor $Q_s = (\omega_s rc)^{-1}$. The
369 reflection coefficient $\Gamma(\omega)$ then reads:

$$370 \Gamma(\omega) = \frac{\left[1 - \left(\frac{\omega}{\omega_s}\right)^2\right] + j \left(\frac{\omega}{\omega_s}\right) Q_s^{-1}(1 - r^{-1})}{\left[1 - \left(\frac{\omega}{\omega_s}\right)^2\right] + j \left(\frac{\omega}{\omega_s}\right) Q_s^{-1}(1 + r^{-1})} \quad (\text{A1})$$

FIG. 12. Bode diagram of the reflection coefficient of a SDOF resonator, with constant quality factor $Q_s=1$ and varying resistances ($r \in [0.1, 10]$)

FIG. 13. Bode diagram of the reflection coefficient of a SDOF resonator, with constant resistance $r=0.3$ and varying quality factors ($Q \in [0.1, 10]$)

371 We first vary the values of the resistance r with a fixed quality factor $Q_s = 1$. The
372 bode diagram of the reflection coefficient is presented in Figure 12. The inspection of the
373 reflection coefficient shows that, for a unitary resonance quality factor, when $r < 1$, the
374 reflection coefficient spans the whole 2π , whereas values of $r > 1$ yield smaller ranges of the
375 reflection coefficient phase. Therefore, the necessity to achieve reflection phases spanning the
376 whole $[0 - 2\pi]$ range motivates the choice of an acoustic resistance lower than Z_c . It is also
377 noticeable that, for values $r \approx 1/3$, the reflection coefficient phase variation varies linearly
378 with frequency on the broadest frequency band. Moreover, since the minimal reflection
379 coefficient value for $r = 1/3$ is $\Gamma = 0.5$, it might be timely to chose values of resistances
380 varying around this value for the whole unit-cells.

381 Then, if we set the resistance $r = 0.3$, we can assess the sensitivity of the reflection
382 phase variation to the quality factor, as illustrated in Figure 13. For a low value of Q_s ,
383 the reflection phase does not span a sufficiently wide range. For a high value of Q_s , the
384 phase variation is linear only over a too narrow frequency band (an objective limit could
385 be one octave). There is then a compromise to find between the different phase profiles
386 (eg. spanning over the whole trigonometric circle vs. bandwidth extension). Then, we have
387 chosen to set $r = 0.3$ and $Q_s = 6$ to allow a wide range of reflection coefficient control over
388 at least one octave.

389 REFERENCES

- 390 ¹S. A. Cummer, J. Christensen, and A. Alù, *Nature Reviews Materials* **1**, 16001 (2016).
391 ²H. Esfahlani, S. Karkar, H. Lissek, and J. R. Mosig, *Scientific reports* **6**, 18911 (2016).
392 ³H. Esfahlani, S. Karkar, H. Lissek, and J. R. Mosig, *The Journal of the Acoustical Society*
393 *of America* **139**, 3259 (2016).
394 ⁴H. Esfahlani, S. Karkar, H. Lissek, and J. R. Mosig, *Physical Review B* **94**, 014302 (2016).

- ⁵X. Wang, D. Mao, and Y. Li, *Scientific Reports* **7** (2017).
- ⁶H. Esfahlani, H. Lissek, and J. R. Mosig, *Physical Review B* **95**, 024312 (2017).
- ⁷A. B. Khanikaev, R. Fleury, S. H. Mousavi, and A. Alù, *Nature communications* **6** (2015).
- ⁸S. Yves, R. Fleury, F. Lemoult, M. Fink, and G. Lerosey, *New Journal of Physics* **19**, 075003 (2017).
- ⁹Y. Li and B. M. Assouar, *Applied Physics Letters* **108**, 063502 (2016).
- ¹⁰Y. Li, B. Liang, Z.-m. Gu, X.-y. Zou, and J.-c. Cheng, *Scientific reports* **3**, 2546 (2013).
- ¹¹C. Faure, O. Richoux, S. Félix, and V. Pagneux, *Applied Physics Letters* **108**, 064103 (2016).
- ¹²N. Jiménez, T. J. Cox, V. Romero-García, and J.-P. Groby, *Scientific Reports* **7** (2017).
- ¹³S. Lani, K. G. Sabra, and F. L. Degertekin, *Journal of Applied Physics* **117**, 045308 (2015), <https://doi.org/10.1063/1.4906549>.
- ¹⁴L. D. Landau, J. Bell, M. Kearsley, L. Pitaevskii, E. Lifshitz, and J. Sykes, *Electrodynamics of continuous media*, Vol. 8 (elsevier, 2013).
- ¹⁵B.-I. Popa, D. Shinde, A. Konneker, and S. A. Cummer, *Phys. Rev. B* **91**, 220303 (2015).
- ¹⁶X. Chen, P. Liu, Z. Hou, and Y. Pei, *Scientific Reports* **7** (2017).
- ¹⁷H. Lissek, R. Boulandet, and R. Fleury, *The Journal of the Acoustical Society of America* **129**, 2968 (2011).
- ¹⁸R. Boulandet, E. Rivet, and H. Lissek, *Acta Acustica united with Acustica* **102**, 696 (2016).
- ¹⁹E. Rivet, S. Karkar, and H. Lissek, *IEEE Transactions on Control Systems Technology* **25**, 63 (2017).
- ²⁰E. Rivet, S. Karkar, and H. Lissek, “On the optimisation of multi-degree-of-freedom acoustic impedances of low-frequency electroacoustic absorbers for room modal equalisation,” (2017), (in Production) in *Acta Acustica united with Acustica*.
- ²¹R. Fleury, D. L. Sounas, and A. Alù, *Phys. Rev. Lett.* **113**, 023903 (2014).
- ²²R. Fleury, D. Sounas, and A. Alù, *Nature communications* **6**, 5905 (2015).
- ²³R. Fleury, D. L. Sounas, and A. Al, *IEEE Journal of Selected Topics in Quantum Electronics* **22**, 121 (2016).
- ²⁴Here we define the acoustic impedance as a ratio between sound pressure and particle velocity, although it is conventionally defined as the ratio between pressure and flow velocity²⁵.
- ²⁵M. Rossi, “Audio,” (Presses Polytechniques Fédérales de Lausanne, 2007) Section 9.1, pp.

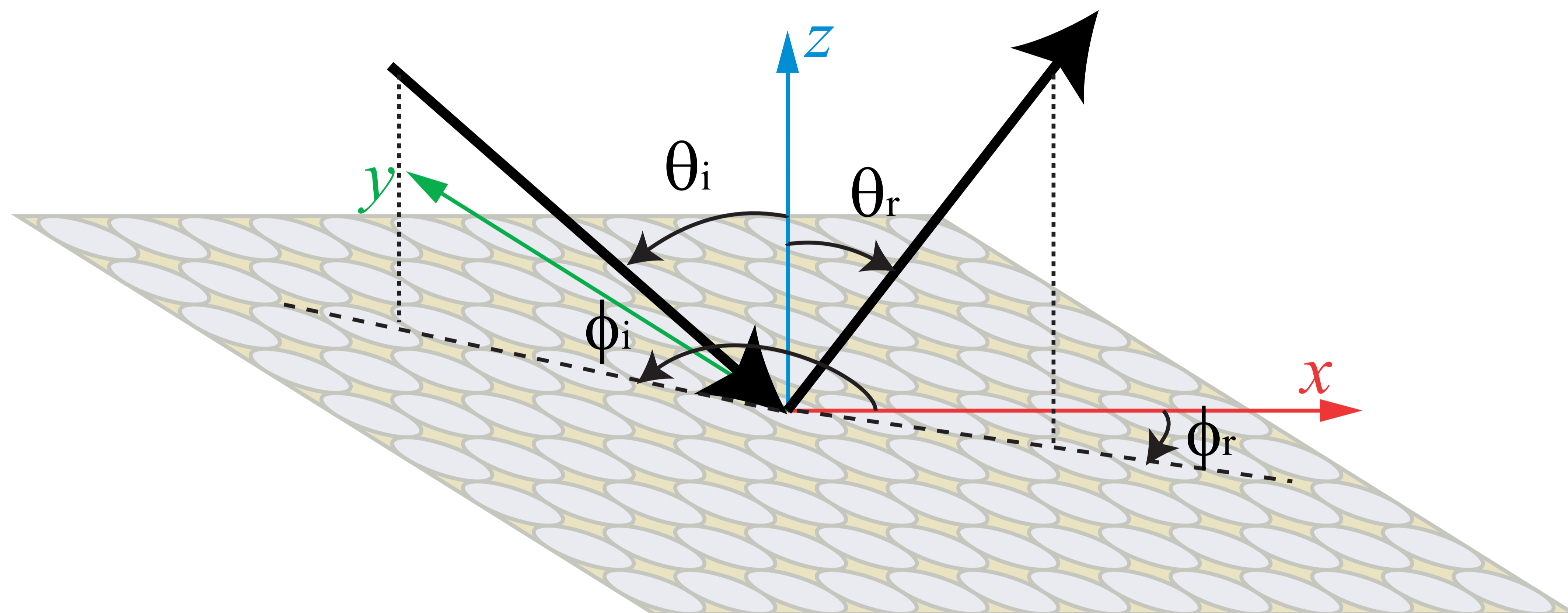
53–540.

428 ²⁶U. Seidel and w. Klippel, in *Audio Engineering Society Convention 110* (2001).

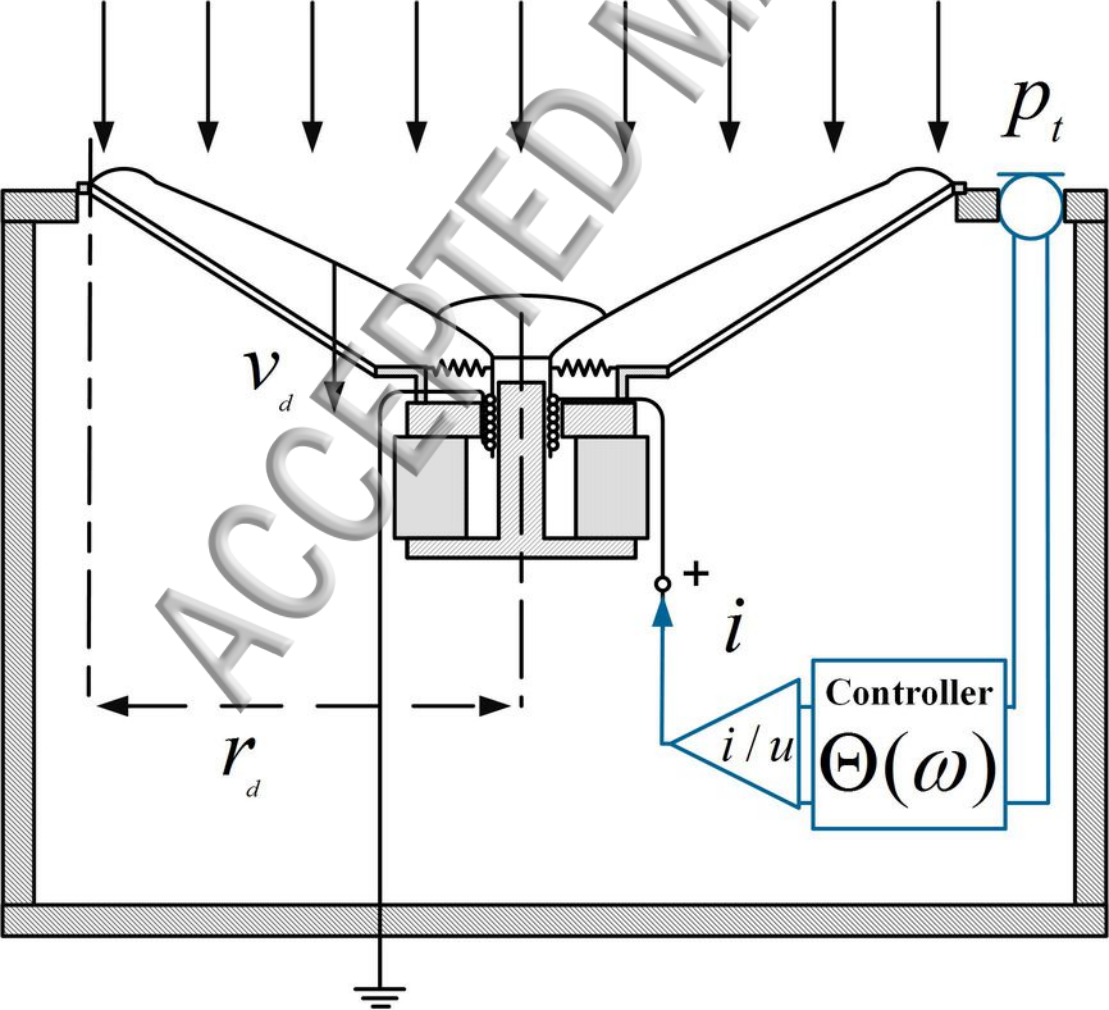
429 ²⁷E. Rivet, *Room Modal Equalisation with Electroacoustic Absorbers*, Ph.D.
430 thesis, Ecole Polytechnique Fédérale de Lausanne (2016), (accessible on
431 <https://infoscience.epfl.ch/record/222866>).

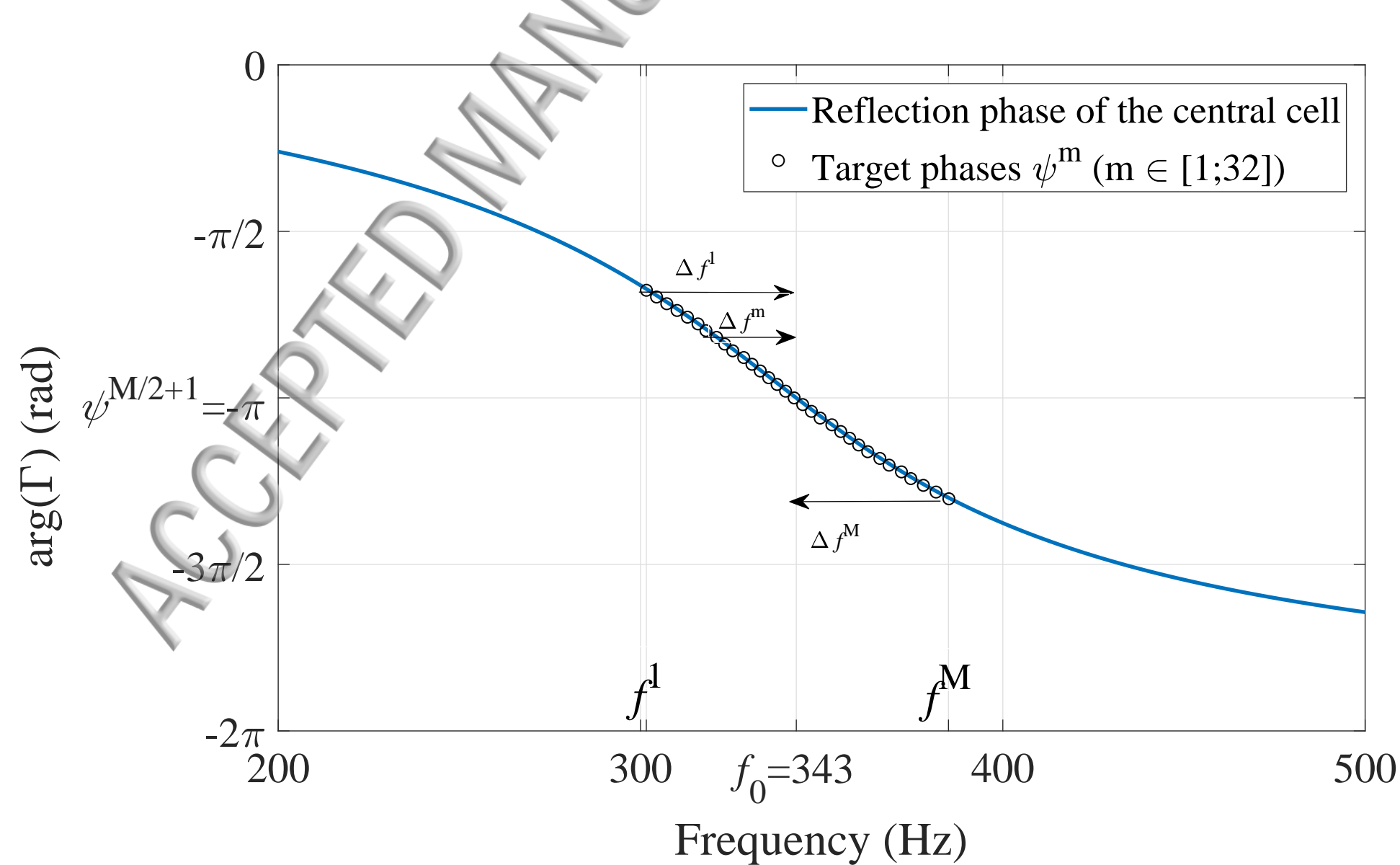
432 ²⁸“Iso 10534-2-1998 : Acoustics - determination of sound absorption coefficient and
433 impedance in impedance tubes - part 2 : Transfer-function method,” ISO, Geneva, Switzer-
434 land (1998).

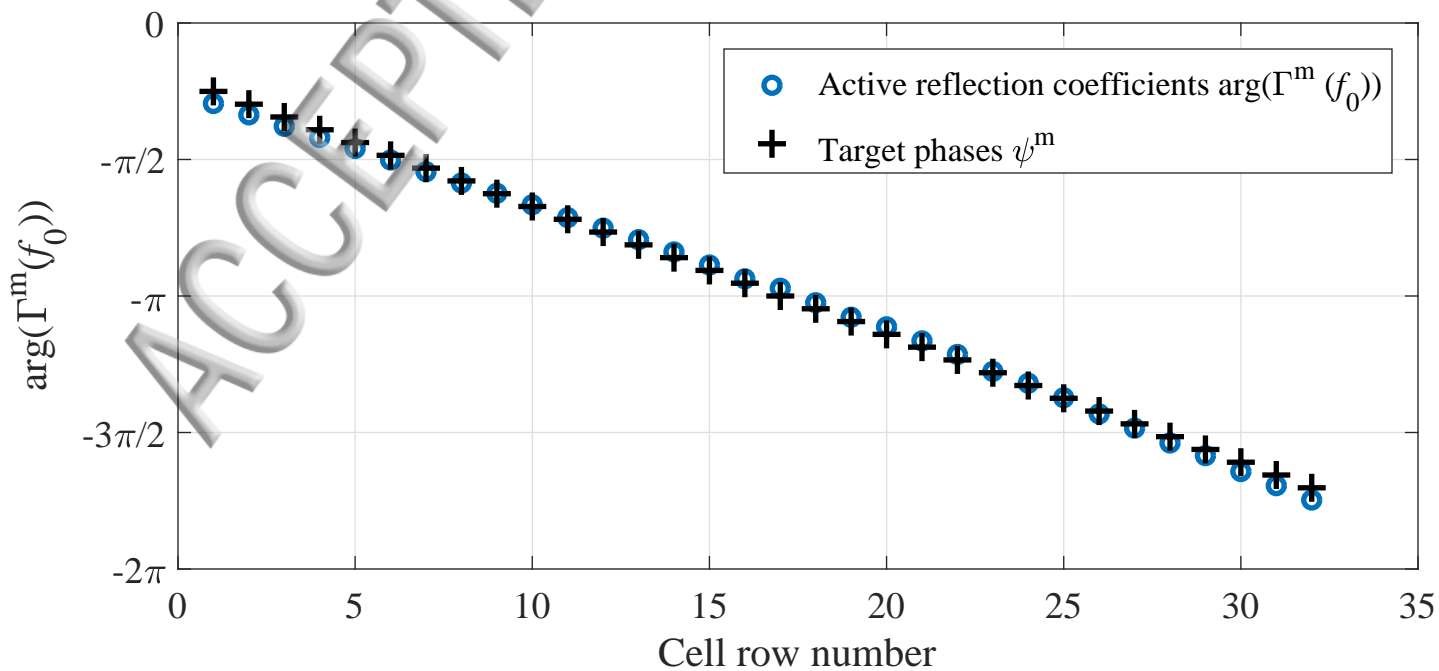
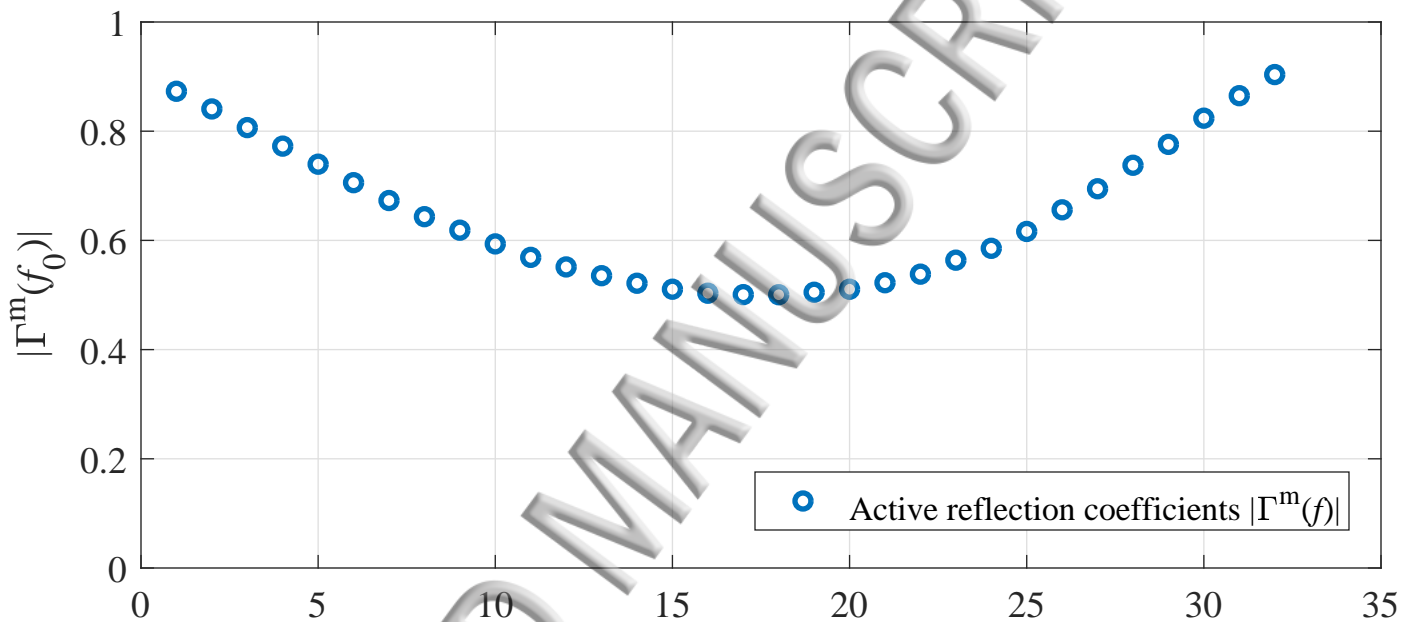
ACCEPTED MANUSCRIPT

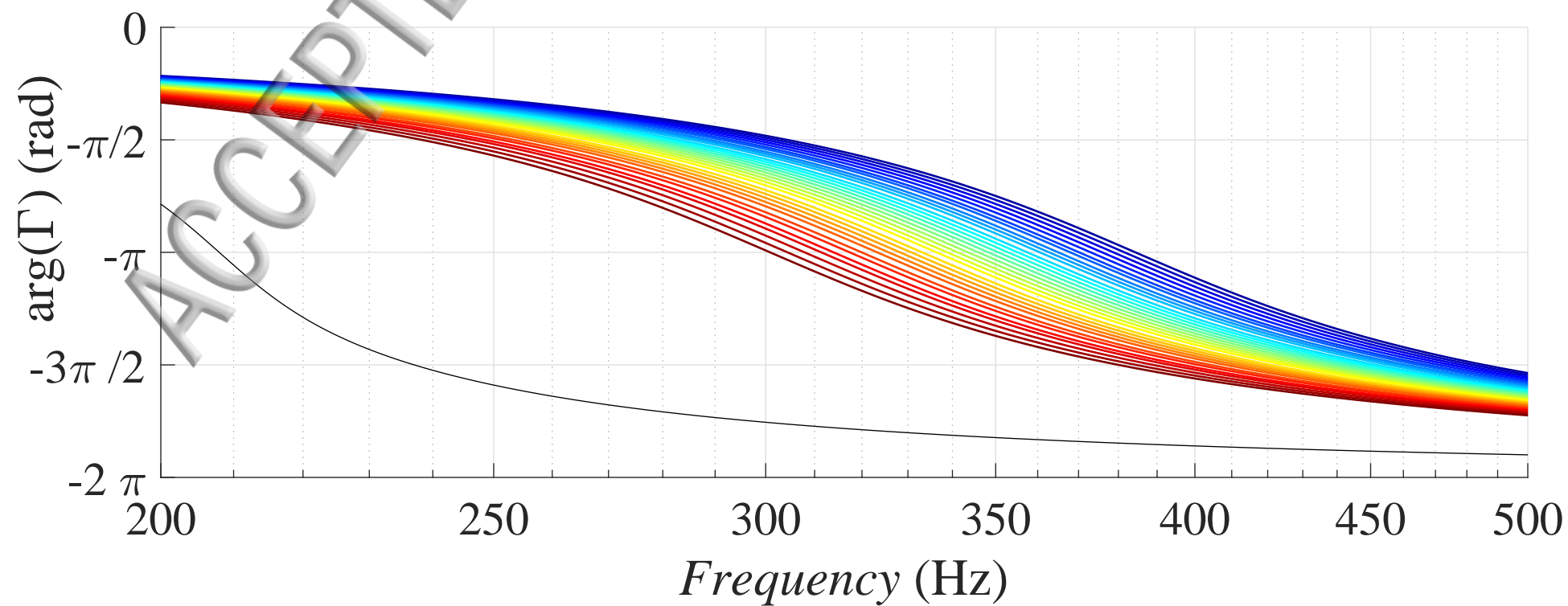
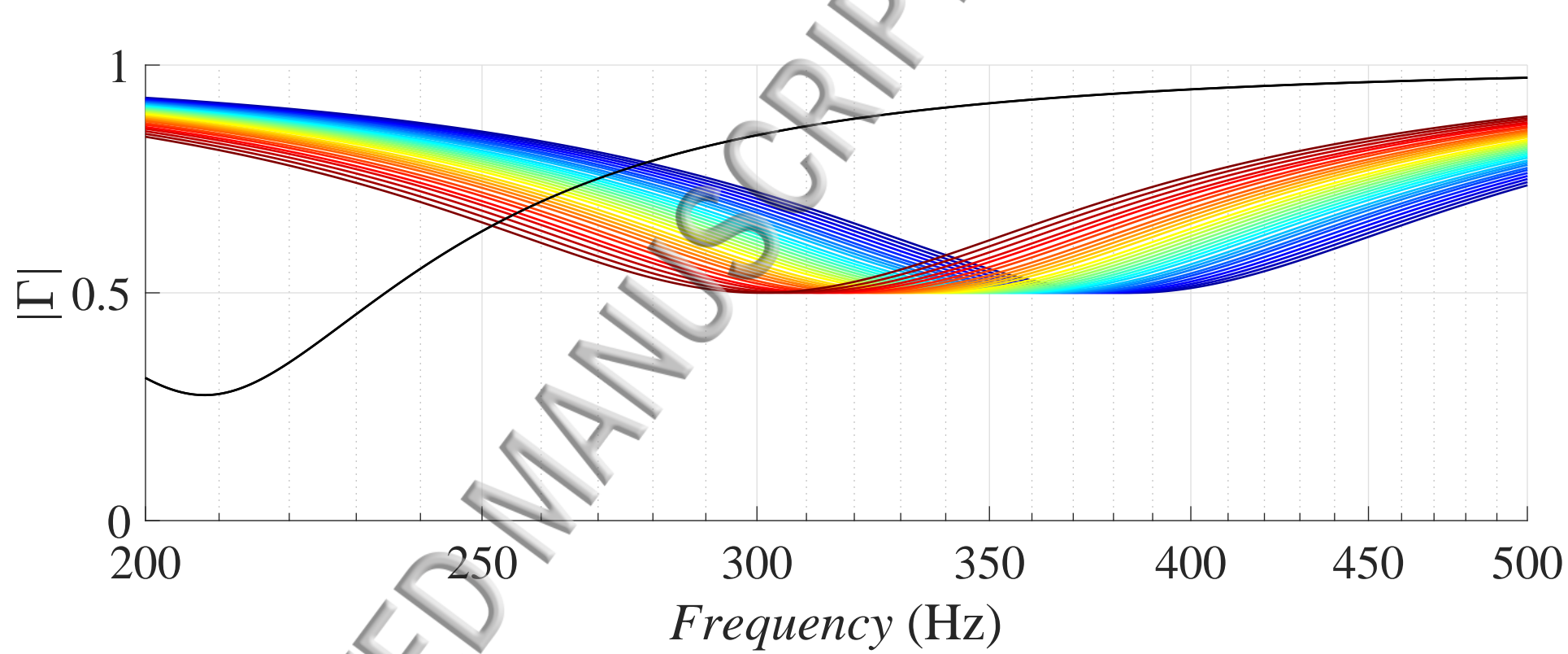


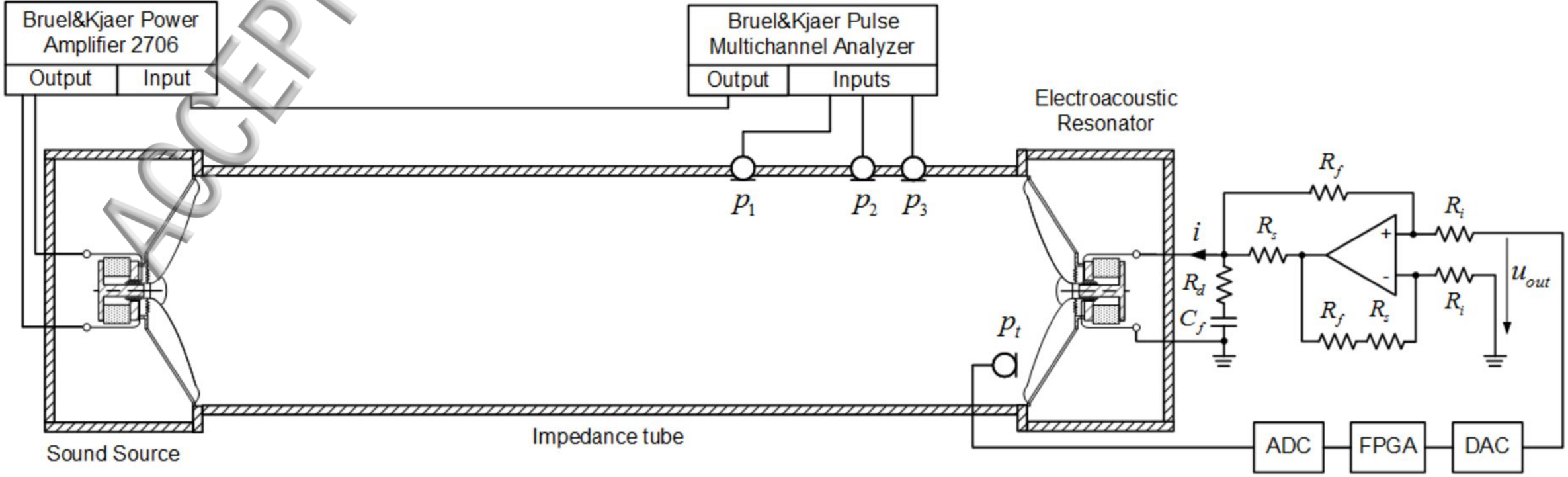
This manuscript was accepted by J. Appl. Phys. Click [here](#) to see the version of record.

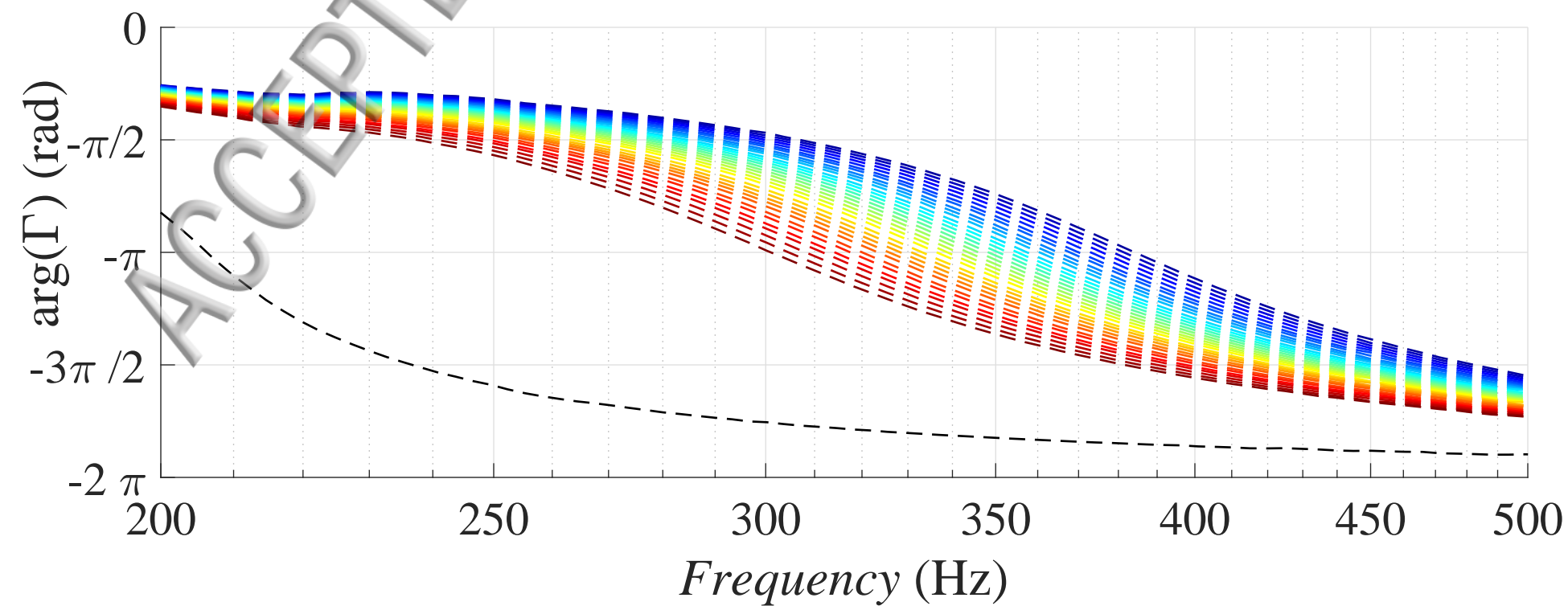
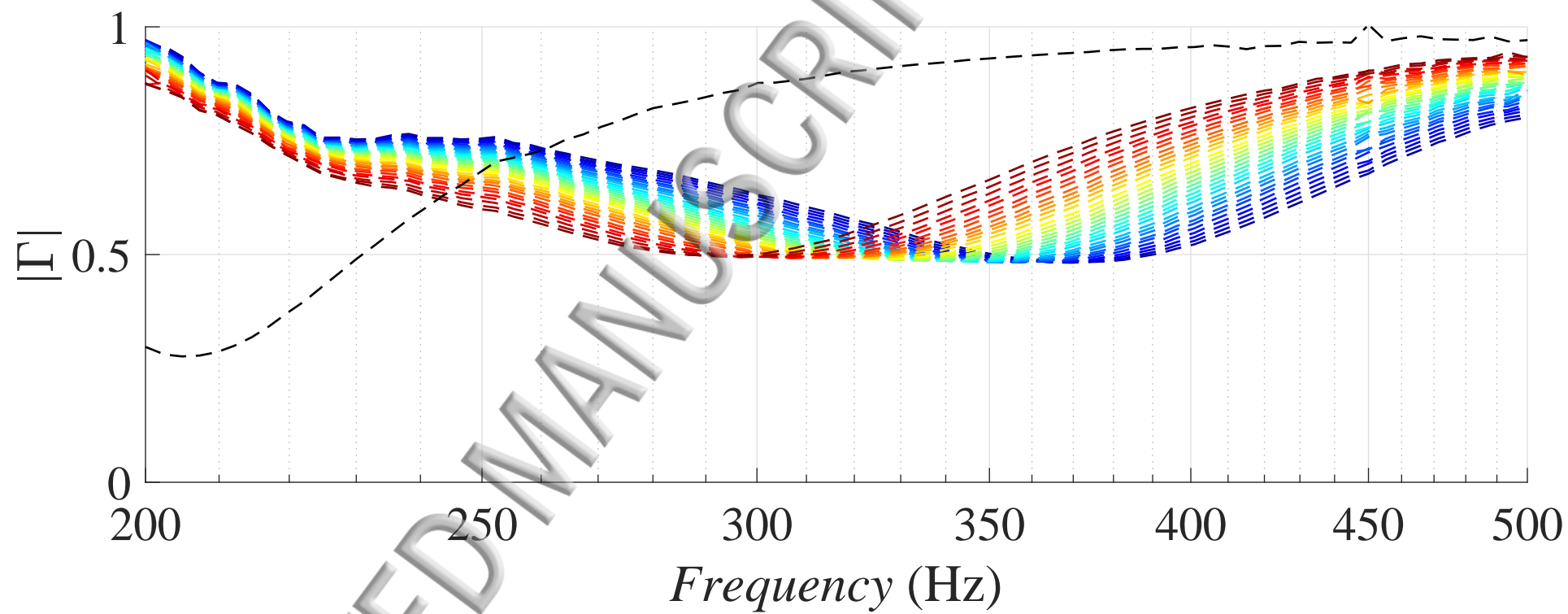




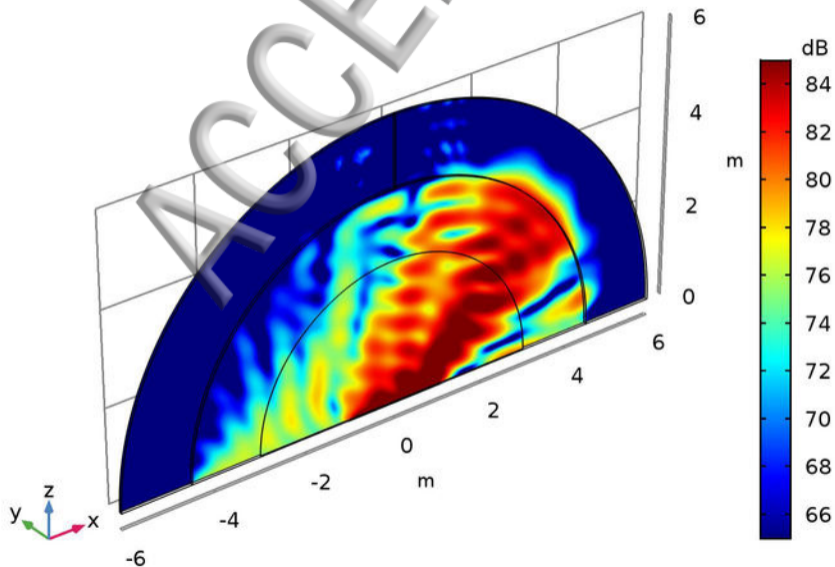




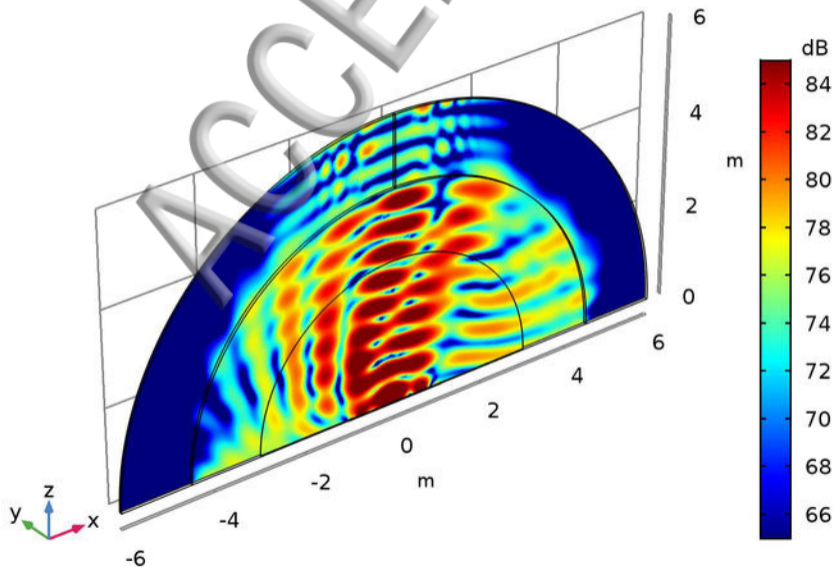


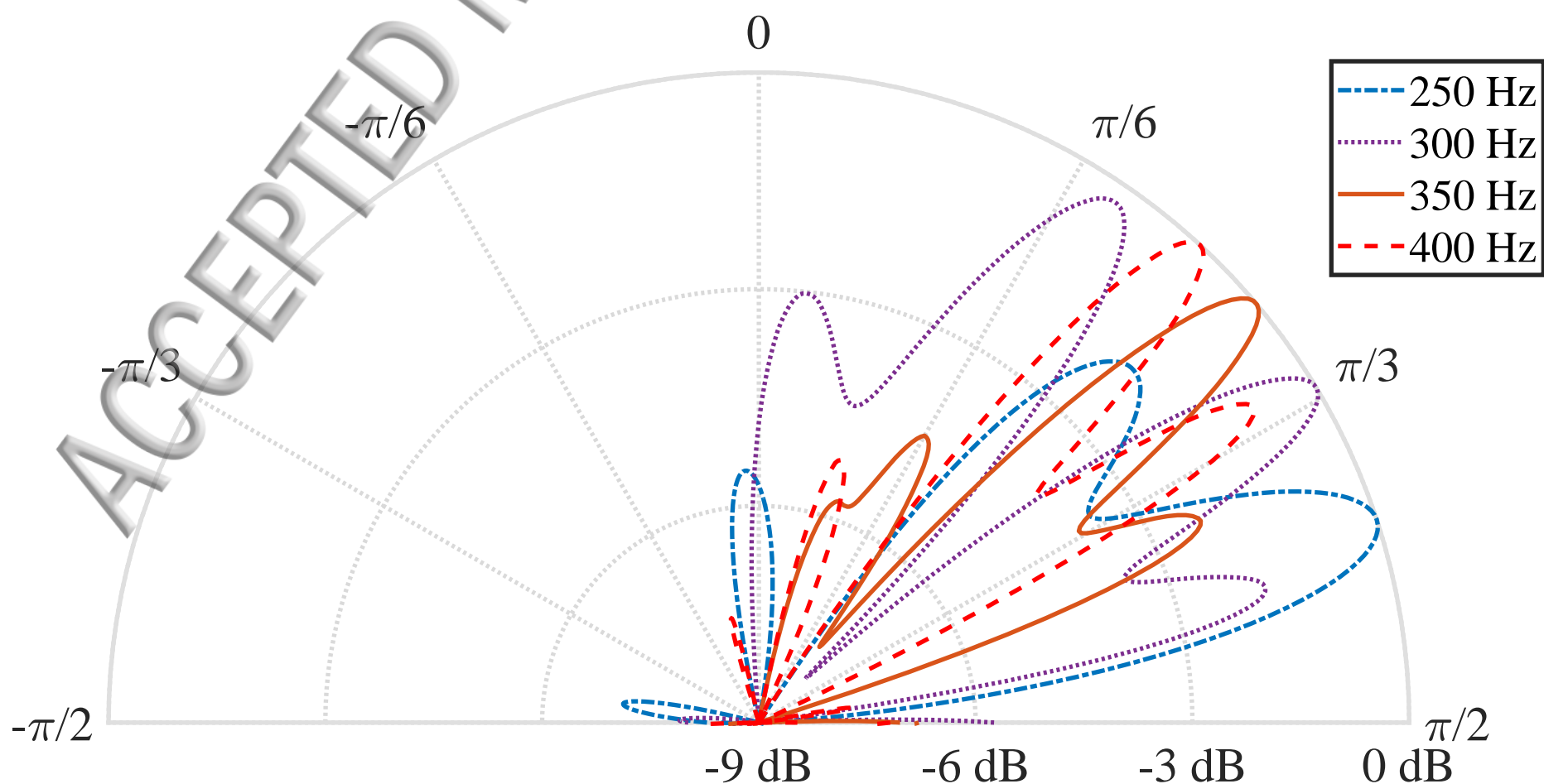


f=350 Hz - Reflected Sound Pressure Levels Map (dB re. 20 μ Pa)



f=350 Hz - Reflected Sound Pressure Levels Map (dB re. 20 μ Pa)





ACCEPTED

